Composite Multiferroic Terahertz Emitter: Polarization Control via an Electric Field

D. Khusyainov,[1] S. Ovcharenko,[1] A. Buryakov,[1,*] A. Klimov,[1] P. Pernod,[3] V. Nozdrin,[2] E. Mishina,[1] A. Sigov,[1] V. Preobrazhensky,[2] and N. Tiercelin[3]

[1] *MIREA - Russian Technological University, Moscow 119454, Russia*

[2] *Prokhorov General Physics Institute of RAS, Moscow 119991, Russia*

[3] *University of Lille, CNRS, Centrale Lille, Université Polytechnique Hauts-de-France, UMR 8520 - IEMN, 59000 Lille, France*

(Received 19 November 2021; revised 4 February 2022; accepted 28 March 2022; published 13 April 2022)

Electrical control of conjugate degrees of freedom in multiferroics provides the advantage of reducing energy consumption to femto- and even attojoules per switch in spintronics and memory devices. This is achieved through the development of technologies that make it possible to fabricate artificial materials with constantly improving properties. Here, we present the design, physics, and characteristics of a composite multiferroic spintronic emitter, which provides electrical control of the emitted terahertz (THz) wave polarization. The effect is due to electrical control of the magnetization in a high-quality magnetostrictive superlattice, $TbCo_2$/Fe-Co, deposited on an anisotropic piezoelectric substrate. In our approach, several mechanisms are realized in the system simultaneously: the strain-mediated coupling of the magnetic and piezoelectric subsystems, which operate in the range of the spin-reorientation transition of the magnetic superlattice, and THz-wave generation in the superlattice by an optical femtosecond pulse. This provides flexibility and control of the set of parameters. We determine the magnetoelectric parameter, which is responsible for THz polarization control. Our results offer a significant fundamental insight into the physics of composite multiferroic systems that can be used for applications of multiferroicity, primarily for THz spintronic emitters. We believe that our findings represent a decisive step towards technologies for other types of spintronic and memory devices.

DOI: 10.1103/PhysRevApplied.17.044025

I. INTRODUCTION

Multiferroics are materials in which several types of coupled order parameters are simultaneously presented: ferroelectricity, ferromagnetism, and ferroelasticity (or ferrotoroidicity) [1]. Among them, magnetoelectric coupling of magnetic and electrical order parameters is the most widespread and studied phenomenon [2–7].

Magnetoelectrics, the history of which dates back to the 19th century, starting with their prediction [8] and implementation [9–11], are now very close to commercial use in various devices [12,13]. One of the most important advantages of magnetoelectric multiferroics is the ability to reduce, by several orders of magnitude, energy consumption for the switching of magnetic states in spintronic and memory devices; this decreases to femto- and even attojoules [14–18]. Despite extensive and intensive development in the last decade of both the physics and technology of magnetoelectric multiferroics [19–28], a window of opportunity remains open for discovering effects that can further expand the field of application and improve the characteristics of devices based on these materials.

Recently, an area of spintronics, terahertz (THz) spintronics, has been intensively developed. This has happened because THz radiation, which, for many years, fell into an unexplored and unused gap in the full electromagnetic spectrum, finally started to be investigated, primarily due to the creation of convenient femtosecond lasers, and showed a huge range of applications [29–34]. Analogously to common (near-visible) optics, THz optics requires a set of THz optical elements to generate, manipulate, and detect THz radiation. Spintronic THz emitters prove to be indispensable in their characteristics due, first of all, to the width of the generated spectrum (0.5–10 THz) and compactness (they have already emerged the market [35]).

A very important task in operating THz radiation is to control its polarization. At present, for this task, THz quartz wave plates are used (and are available on the market [36]). However, the absorption of quartz is quite strong in the THz range, particularly for frequencies higher than 3 THz. In addition to unwanted losses, this means that the THz radiation transmitted through the half-wave

*buryakov@mirea.ru

plate intrinsically has an irreducible elliptical polarization component.

An efficient way to control polarization is provided by spintronic emitters. They allow for control of the polarization directly during THz generation: switch the phase, rotate the polarization, or even adjust the polarization in a more sophisticated way [37]. Recent results show the possibility of coherent control of asymmetric spintronic terahertz emission [38]. Since the polarization of the terahertz wave is perpendicular to the magnetization of the spintronic emitter, the magnetization should be rotated to rotate the polarization. Initially, the idea of mechanical rotation of a magnet around the emitter was proposed [39]. Then an emitter was developed that rotated the polarization by simply increasing-decreasing the current in the electromagnet [40]; the operation is based on a spin-reorientation phase transition in magnetic nanostructures. In Ref. [41], an alternating magnetic field was applied to scan the THz polarization direction. The current trend, driven by the requirements for energy efficiency and compactness of devices, is to replace current-controlled systems with voltage-controlled ones [42]. The use of a composite multiferroic is a way to combine the advantages of spintronic THz emission and voltage control.

Here, we present the design and characteristics of a composite multiferroic spintronic emitter, which provides electric control of polarization of the emitted THz wave in the range up to 66°. To integrate the spintronic principle of emission with the multiferroic concept of controlling the magnetization by an electric field, we use a high-quality magnetostrictive superlattice deposited on an anisotropic piezoelectric substrate, while the THz wave is generated in the superlattice by an optical femtosecond pulse. The principle of polarization control in such a structure is based on the strain-mediated coupling of magnetic and piezoelectric subsystems in the range of the spin-reorientation transition [17,18,40]. By comparison of the experimental results with the theoretical model, we determine the parameter of magnetoelectrically induced anisotropy, which is responsible for the rotation of the magnetization and THz polarization.

II. METHODS

$Pb(Mg_{1/3}Nb_{2/3})_{0.7}Ti_{0.3}O_3$ (PMNPT) single-crystal substrates are commercial (011)-cut and one-side polished with a size of $5 \times 5 \times 0.3$ mm^3. ($TbCo_2$ 4.4 nm/Fe-Co 5.2 nm) $\times$ 25 multilayers with the total thickness of 240 nm are deposited on top of the substrate by rf sputtering. Sputtering is performed in a constant magnetic field, which induces the magnetic anisotropy of the "easy axis" type in the film plane. The easy axis is directed at an angle of 45° relative to the [100] crystallographic axis of the PMNPT substrate. Sputtering details are given in note 3 within the Supplemental Material [43].

Magnetic properties of the samples are studied using a vibration magnetometer (ADE EV9, MicroSense) with a resolution of $1 \div 5$ μemu. The results are presented in Fig. S3 within the Supplemental Material [43].

For THz time-domain spectroscopy (TDS), an amplified femtosecond laser system is used with a laser pulse duration of 35 fs, wavelength of 800 nm, a pulse repetition rate of 3 kHz, and a pulse fluence of up to 1.8 mJ/cm^2. Details are given in note 1 within the Supplemental Material [43].

III. RESULTS

THz emission is generated by a linearly polarized femtosecond laser pulse incident at 45° onto a multiferroic composite structure. The structure consists of a magnetic ($TbCo_2$/Fe-Co) $\times$ 25 superlattice, which is deposited onto a PMNPT ⟨011⟩ piezoelectric substrate. A schematic view of the structure and the configuration of magnetization and external fields regarding the magnetocrystalline axes are presented in Fig. 1(a). Magnetic hysteresis loops measured in two perpendicular directions unambiguously demonstrate an in-plane anisotropy with an anisotropy field of $H_A = 1.4$ kOe (see Fig. S3 within the Supplemental Material [43]). To achieve the maximum and controlled rotation of the THz-wave polarization when a voltage is applied to the substrate, the sample is mounted in such a way that the direction of the hard axis of magnetic anisotropy coincides with the direction of the magnetic field. A detailed sample description and the scheme of the optical experiment are presented in Sec. II.

The temporal waveform and appropriate spectrum of the generated THz pulse are shown in Fig. 1(b). The measurements are performed on the substrate at a voltage of 60 V and a magnetic field of 0.7 kOe, which provides a maximal signal for each fixed pump fluence. The maximal spectral amplitude is observed at a frequency of 0.8 THz, and the spectral bandwidth is limited to 3.5 THz due to the spectral range of the detector. The THz pulse peak-to-peak signal linearly depends on the fluence of the optical pump [Fig. 1(c)].

In the THz $TbCo_2$/Fe-Co emitter, a change in the absolute value of the magnetic field below the anisotropy field, H_A, rotates polarization [40]. When all optical components are fixed, the Zn-Te-based detection system acts as an optical analyzer measuring the E_y-THz-field component [44–46]. This gives a THz-amplitude hysteresis loop when the magnetic field is swept [Fig. 2(a)]. The slopes of the hysteresis loops are opposite because the magnetization deviates in opposite directions from the y axis under a voltage of the opposite sign [see Fig. 1(a)]. If the electric field rotates polarization, analogous THz-amplitude hysteresis loops should be observed when the electric field is swept. This is exactly what is obtained in our measurements [Fig. 2(b)].

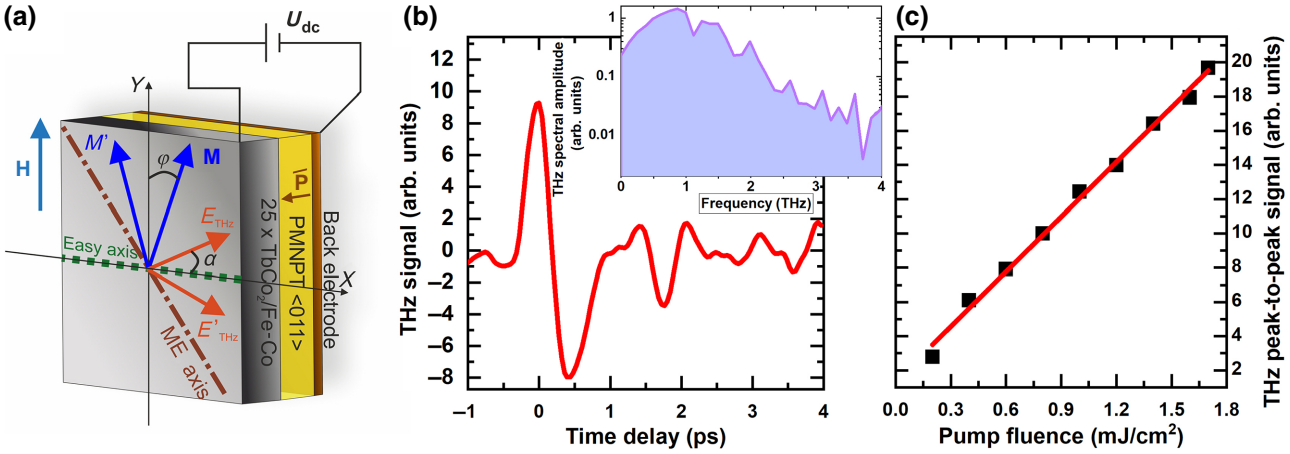

FIG. 1. Sample structure and THz pulse characterization. (a) Scheme of the composite multiferroic emitter: orientation of the axes of magnetocrystalline (easy axis) and magnetoelastic (ME axis) anisotropy, external magnetic field **H**, magnetization **M**, THz-wave electric field **E**; $\bar{\mathbf{P}}$, ferroelectric crystal polarization axis normal to the structure plane; φ, the angle between magnetization **M** and the hard axis ($\varphi = \alpha$). Back electrode is made of copper. (b) Temporal waveform and spectrum (inset) of the generated THz pulse. (c) Dependence of THz peak-to-peak amplitude on the pump fluence.

From Fig. 2, the electric field and magnetic field look interchangeable: sweeping of both gives hysteresis loops for the amplitude of the THz field. But this is not the exact case: for $H = 0$, no THz signal is observed at all for any voltage [Fig. 2(b), light brown line]. At the same time, small splashes of THz field are observed for $U = 0$, $H = 1$ kOe, when the magnetic field is swept [Fig. 2(a), green line]. The width of the magnetic hysteresis loop for the THz amplitude can be determined by $H_{loop} = \pm 1$ kOe. The width of the electric hysteresis loop for the THz amplitude can be determined by $U_{loop} = \pm 60$ V. The value of 60 V is found to be the optimal voltage that provides the maximal THz amplitude. This is found through the direct measurements of the THz signal on the electric field. As shown in Fig. S4 within the Supplemental Material [43], the polarization-angle-control range decreases sharply above 60 V. This is due to a sharp decrease, above this limit, of piezoelectric deformation in the PMNPT ⟨011⟩ ferroelectric crystal [30]. This limit in our sample corresponds to an electric field of 0.2 MV/m.

The value of the polarization rotation angle in the scheme used can be obtained only by complete polarization measurements when the THz field polarizer is rotated (see note 1 within the Supplemental Material [43]). From these types of measurements, we first confirmed the pure rotation of polarization without any change in the amplitude of THz radiation for the range of the magnetic field, $|H| < 3$ kOe and $U = 0$.

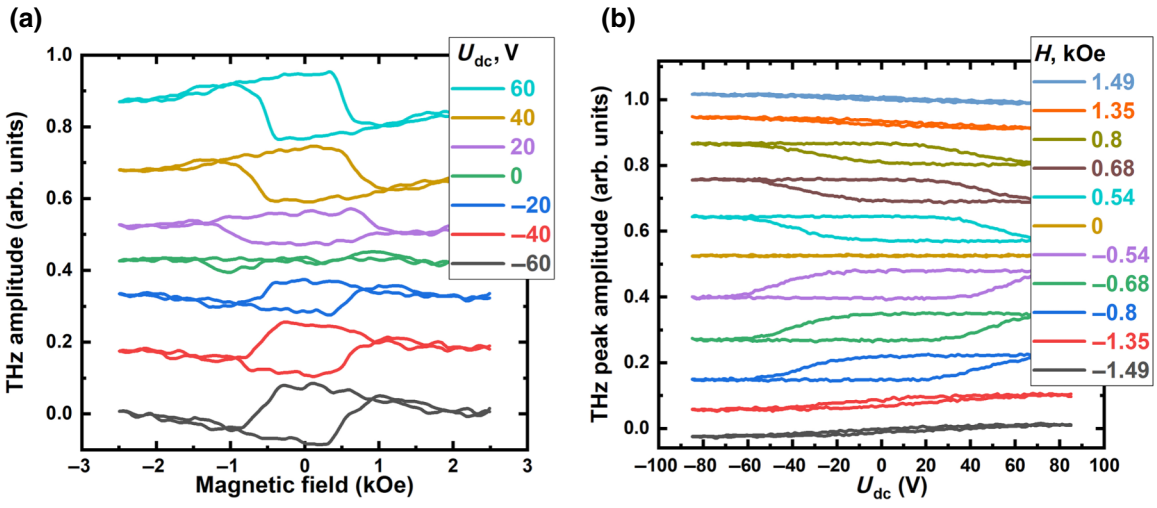

FIG. 2. Dependences of the THz amplitude E_y (a) on the magnetic field strength for different voltages and (b) on the voltage for different values of magnetic field strength (THz-amplitude magnetic and electric hysteresis loops, respectively).

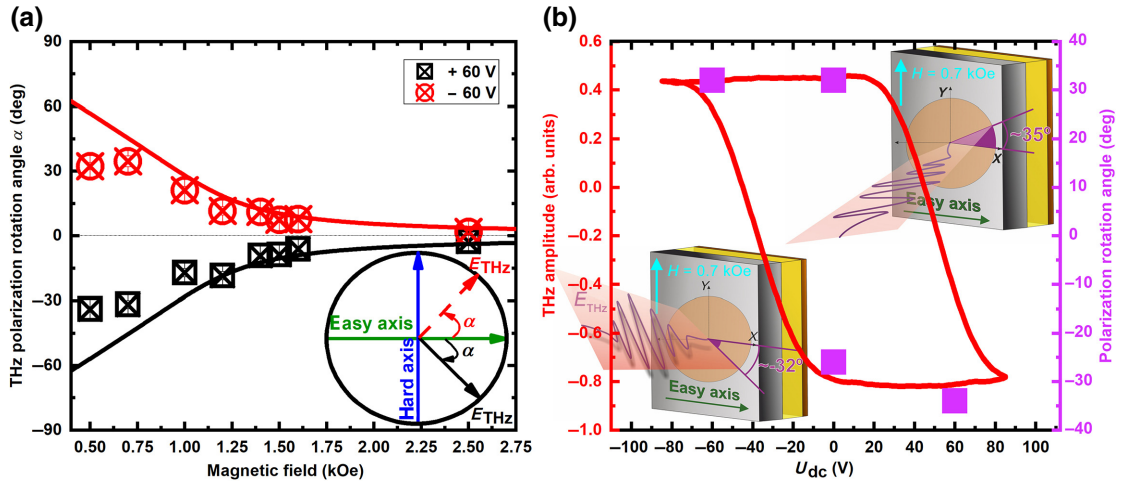

FIG. 3. THz polarization rotation (a) α versus magnetic field applied along the hard axis at a substrate voltage of 60, −60 V. Line corresponds to theoretical calculation. Inset, THz polarization angle at two different angular regions relative to the easy axis direction. (b) α versus voltage applied to the substrate at a fixed magnetic field of 0.7 kOe (points, right scale) and corresponding maximum amplitude of the THz pulse (line, left scale).

Then, the voltage of 60 V is set and the polarization rotation angle, α, is measured as a function of magnetic field [Fig. 3(a)]. The maximal value of α is observed at $H = 0.7$ kOe and decreases rapidly up to $H = 1.5$ kOe, followed by a very slow decrease for a stronger magnetic field (which corresponds to a saturation of magnetization at $U = 0$).

Rotation of polarization reverses direction when the sign of the electric field is reversed [see inset in Fig. 3(a)], showing an odd voltage dependence, $\alpha(-U) = -\alpha(U)$. The latter allows the total rotation to be doubled, which reaches 66° in the experiment.

Figure 3(b) demonstrates the operation principle of polarization switching and the correlation between the electric hysteresis loop of the THz-emission amplitude and polarization rotation angle for the optimal conditions found. Polarization switching is accompanied by a change in the sign of the THz pulse, but without a change in the amplitude value. Notably, the THz amplitude is measured directly at the maximum of the THz signal by scanning the value of U_{dc} of the dc voltage on PMNPT. The polarization rotation angle is the result of the fitting of polarization dependences for specific U_{dc} values (see note 2 within the Supplemental Material [43]).

Figure 4 shows the dependence of the maximum THz-pulse amplitude on magnetic field (THz magnetic hysteresis loop). The sample can be rotated around the normal to the surface (azimuthally). When a magnetic field is applied exactly along the hard axis, the dependence of the THz amplitude on the magnetic field degenerates [Fig. 4(a)], except for small peaks at a field of $H = \pm 1$ kOe. Azimuthal rotation by 4° from the direction of

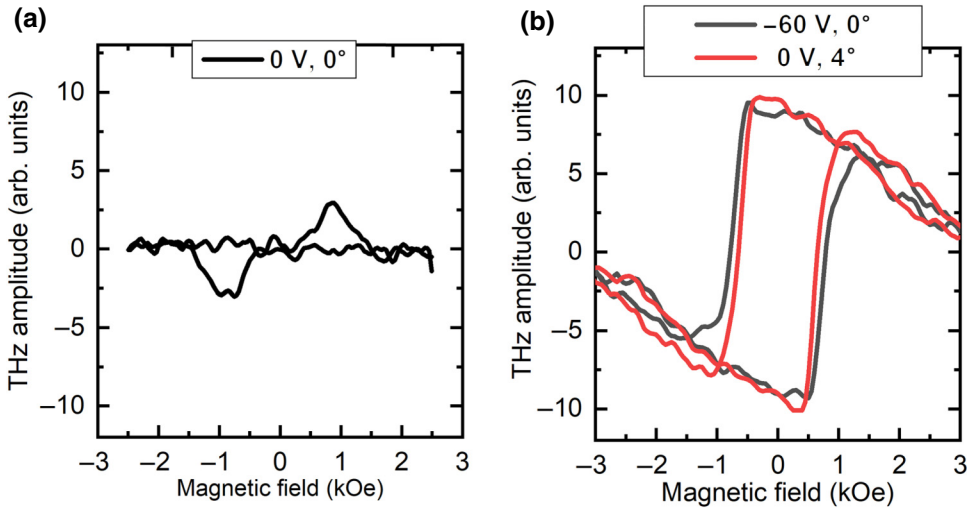

FIG. 4. Interchangeability of voltage and azimuthal sample position. Dependences of the maximum THz pulse amplitude on magnetic field for (a) zero voltage and exact hard-axis orientation; (b) two azimuthal sample positions (0, 4°) and two values of applied voltage (0 and −60 V). Delay time is fixed at $t = 0$ ps.

the hard axis leads to a significant increase of the THz-emission amplitude and the appearance of its ordinary hysteresis dependence on the magnetic field [Fig. 4(b), black line]. Application of a voltage to the PMNPT substrate also removes the degeneracy. For the voltage of −60 V and exact orientation of the hard axis along the magnetic field [zero azimuthal angle, red line in Fig. 4(b)], the two hysteresis loops coincide with each other. Thus, we observe the interchangeability of voltage application to the PMNPT substrate and the azimuthal rotation of the sample relative to the direction of the magnetic field.

IV. MODEL AND DISCUSSION

According to the mechanism of inverse spin-Hall effect, the polarization of THz radiation is orthogonal to the spin current polarization, which is parallel to the magnetization. In the strain- mediate composite multiferroic, the application of an electric field to the ferroelectric layer generates elastic deformation in the magnetic subsystem. Specific symmetry of the PMNPT ⟨011⟩ crystal provides anisotropic in-plane deformation under electric field normal to the structure. Due to the effect of magnetostriction, this deformation causes uniaxial magnetoelastic anisotropy in the plane of the intermetallic multilayer. For a reason of the magnetic multilayer deposition in a magnetic field of a certain direction, the angle between the axes of magnetocrystalline and magnetoelastic anisotropy is 45°, as shown in Fig. 1. The thermodynamic potential of the magnetic system as a function of the angle φ between the magnetization **M** and the hard axis of the magnetocrystalline anisotropy contains Zeeman energy of the magnetization interaction with the magnetizing field **H**, the energy of magnetocrystalline anisotropy with effective field H_A, and magnetoelastic anisotropy energy caused by piezoelectric deformation u_{xy}:

$$F(\varphi) = -MH\cos\varphi - \frac{1}{2}MH_A\sin^2\varphi + Bu_{xy}\sin 2\varphi, \quad (1)$$

where B is magnetoelastic constant.

In the absence of deformations, the application of a sufficiently strong magnetic field $H > H_A$ provides the only minimum of the thermodynamic potential at $\varphi = 0$, which corresponds to the saturation magnetization along the hard axis of anisotropy. Decreasing the magnetic field $H < H_A$ creates two equivalent minima for $\cos\varphi = H/H_A$, symmetric with respect to $\varphi = 0$. These two energetically equivalent states bring to the formation of domain structure with opposite projection of the magnetization onto the easy axis. Such structure was visualized in a similar object in the Ref. [47] Emergence of domains is reflected in degeneration of the THz signal shown in Fig. 4 (0 V, 0 deg). The deviation of the magnetic field from the hard axis by a sufficiently large angle leaves only one minimum of the thermodynamic potential, thus the spin reorientation in decreasing magnetic field occurs. This fact is reflected in Fig. 4 (0 V, 4 deg). The effect of magnetoelastic anisotropy is equivalent to the deviation of the easy axis from the normal to the magnetic field as it is seen in Fig. 4(b) (−60 V, 0°).

The effect of strain on the magnetization orientation is carried out through the parameter $V_s = 2Bu_{xy}/(MH_A)$. The physical meaning of the control parameter V_S is the ratio of the energies of strain induced and magnetocrystalline anisotropies. The sign and value of the deformations are controlled by the electric voltage applied to the ferroelectric layer.

The parameter V_s directly determines the deviation angle, θ, of the easy axis: $tg2\theta = 2V_s$. Comparing data in Fig. 4(b), we determine the deviation angle equal to $\theta = 4°$ for an electric field of 0.2 MV/m, which gives $V_S = 0.07$. Within the linear piezoelectric effect, the control parameter is expressed as $V_s = B(d_{32} - d_{31})e_3/(MH_A)$, where d_{3q} are piezoelectric constants and e_3 is the normal projection of the applied electric field. Using the reported parameters of the structure's constituents, $B = -7$ MPa [48], $4\pi M = 8$ kGs (see Fig. S3 within the Supplemental Material [43]), $H_A = 1$ kOe, $d_{32} - d_{31} = -2.5 \times 10^{-9}$ C/N [49], and $e_3 = 0.2$ MV/m, we estimate $V_S = 0.055$, which is close to the measured value.

Figure 5 demonstrates the effect of piezoelectric strain on the thermodynamic potential for two characteristic values of magnetizing field applied normally to the magnetocrystalline easy axis. The magnetic field dependence of the angle φ_m, corresponding to the absolute minimum of

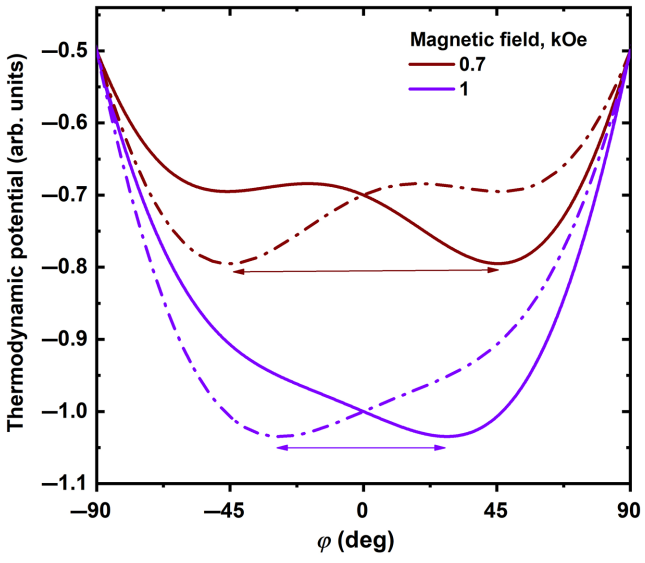

FIG. 5. Magnetization switching between two minima. Thermodynamic potential of the magnetic subsystem at a magnetic field strength $H = H_A = 1$ kOe and $H = 0.7$ kOe when applying a voltage of −60 V (solid lines) and +60 V (dashed-dotted lines).

the thermodynamic potential, is shown in Fig. 3(a) by the lines.

Calculations are performed for a voltage of 60 V using the anisotropy field of the structure, $H_A = 1$ kOe. This value is obtained from data in Fig. 3 as a field of spin-reorientation instability peak for zero deviation angle and zero tension. We should note that this value is about 35% less than that measured by magnetometry (see Fig. S3 within the Supplemental Material [43]). This difference is explained by the effect of anisotropy disruption during optical pumping, as studied previously on a similar intermetallic structure [50].

The thermodynamic potential in the area of spin reorientation, $H < 0.7$ kOe, has two minima, in spite of piezoelectric deformation. The domain structure arises in this area, which is the reason why the measured value of the angle of rotation of polarization is less than that predicted in the framework of the single-domain model. Nevertheless, it is sufficient for THz-polarization control by an electric field over a wide range of 66°.

We note that the thickness of our magnetostrictive multilayer is not optimized in terms of THz-emission efficiency. For the reflection mode of emission used in this work, the choice of thickness is not crucial. We have already reported on THz-emission control by a magnetic field in transition mode in a 26-nm-thick $TbCo_2$/Fe-Co multilayer [40], which is an order of magnitude thinner that that used in this work. However, for polarization control via an electric field, the optimization problem requires special consideration. In contrast to conventional three-layer spintronic emitters, the optimization of a composite multiferroic device should include requirements for the intensity of the THz emission as well as for controllability of the THz polarization. The latter is determined by magnetostriction, depending on the thickness of the structure.

V. CONCLUSION

We report on electric field control over the magnetization direction and, therefore, on the control over the THz-wave polarization without changing the THz-pulse amplitude. We propose a technique for the experimental determination of the strain-induced parameter, V_S, which is responsible for magnetoelectric control of THz polarization. We establish a fundamental relationship between the applied electric voltage and the angle of reorientation of the magnetic anisotropy axis caused by the magnetoelectric effect. It allows us to directly measure (without any fitting or use of unknown material characteristics) the magnetoelectric parameter of THz polarization and to control the magnetization with an electric field. For the studied $TbCo_2$/Fe-Co/PMNPT structure, the measured value of the magnetoelectric parameter is equal to $V_S = 0.07$ for an electric field of 0.2 MV/m.

The polarization-controlling THz spintronic emitter reported here has two advantages over the previously suggested use of a composite structure based on an amorphous magnetic film [42]. First of all, it is based on the $TbCo_2$/Fe-Co magnetic multilayer with a spin-reorientation transition. If a magnetic structure is used as the emitter itself, then polarization control can be provided by changing only the value (not direction) of the magnetic field (as we demonstrated in Ref. [40]). It is very important that the amplitude of the THz wave and its polarization rotation angle are decoupled within the range of spin reorientation transition: pure rotation is achieved with constant amplitude. If the magnetic multilayer is a part of a multiferroic structure, the same is achieved by electric field control. As in the previous case, amplitude and polarization rotation remain decoupled. Second, the observed value of the maximum angle of THz polarization rotation by the electric field is 66°. This is twice that previously reported. The limitation of the polarization-control range, in comparison with the calculated value, is explained by the appearance of a magnetic domain structure in a weak magnetizing field. The current operation voltage is quite high, but it is more than 3 times smaller than that previously used [42]. Moreover, it is expected to be reduced to the commercial battery tension by reducing the technologically induced magnetic anisotropy and by reducing the PMNPT layer thickness with the use of modern nanoelectromechanical systems technologies [51,52].

ACKNOWLEDGMENTS

The work is supported by Russian Science Foundation (Grant No. 20-12-00276). Fabrication of the samples was performed in the frame of French RENATECH network.

[1] W. Eerenstein, N. D. Mathur, and J. F. Scott, Multiferroic and magnetoelectric materials, Nature **442**, 759 (2006).
[2] N. A. Spaldin and R. Ramesh, Advances in magnetoelectric multiferroics, Nat. Mater. **18**, 203 (2019).
[3] Z. Zhou, S. Zhao, Y. Gao, X. Wang, T. Nan, N. X. Sun, X. Yang, and M. Liu, The memory effect of magnetoelectric coupling in FeGaB/NiTi/PMN-PT multiferroic heterostructure, Sci. Rep. **6**, 20450 (2016).
[4] Y. Ba, S. Zhuang, Y. Y. Zhang, Y. Wang, Y. Gao, H. Zhou, M. Chen, W. Sun, Q. Liu, G. Chai, J. Ma, Y. Y. Zhang, H. Tian, H. Du, W. Jiang, C. Nan, J.-M. Hu, and Y. Zhao, Electric-field control of skyrmions in multiferroic heterostructure via magnetoelectric coupling, Nat. Commun. **12**, 322 (2021).
[5] Z. Hu, *et al.*, Non-volatile ferroelectric switching of ferromagnetic resonance in NiFe/PLZT multiferroic thin film heterostructures, Sci. Rep. **6**, 32408 (2016).
[6] Y. Iguchi, Y. Nii, and Y. Onose, Magnetoelectrical control of nonreciprocal microwave response in a multiferroic helimagnet, Nat. Commun. **8**, 15252 (2017).

[7] M. Fiebig, Revival of the magnetoelectric effect, J. Phys. D: Appl. Phys. **38**, R123 (2005).

[8] P. Curie, Sur La symétrie dans Les phénomènes physiques, symétrie d'un champ Électrique et d'un champ magnétique, J. Phys. Theor. Appl. **3**, 393 (1894).

[9] G. A. Smolenskiĭ and I. E. Chupis, Ferroelectromagnets, Sov. Phys. Usp. **25**, 475 (1982).

[10] G. T. Rado and V. J. Folen, Observation of the Magnetically Induced Magnetoelectric Effect and Evidence for Antiferromagnetic Domains, Phys. Rev. Lett. **7**, 310 (1961).

[11] V. J. Folen, G. T. Rado, and E. W. Stalder, Anisotropy of the Magnetoelectric Effect in Cr_2O_3, Phys. Rev. Lett. **6**, 607 (1961).

[12] S. Shevlin, Multiferroics and the path to the market, Nat. Mater. **18**, 191 (2019).

[13] A. Barman, *et al.*, The 2021 magnonics roadmap, J. Phys. Condens. Matter **33**, 413001 (2021).

[14] K. Roy, S. Bandyopadhyay, and J. Atulasimha, Hybrid spintronics and straintronics: A magnetic technology for ultra Low energy computing and signal processing, Appl. Phys. Lett. **99**, 063108 (2011).

[15] R.-C. Peng, J.-M. Hu, L.-Q. Chen, and C.-W. Nan, On the speed of piezostrain-mediated voltage-driven perpendicular magnetization reversal: A computational elastodynamics-micromagnetic phase-field study, NPG Asia Mater. **9**, e404 (2017).

[16] A. Klimov, N. Tiercelin, Y. Dusch, S. Giordano, T. Mathurin, P. Pernod, V. Preobrazhensky, A. Churbanov, and S. Nikitov, Magnetoelectric write and read operations in a stress-mediated multiferroic memory cell, Appl. Phys. Lett. **110**, 222401 (2017).

[17] Y. Dusch, N. Tiercelin, A. Klimov, S. Giordano, V. Preobrazhensky, and P. Pernod, Stress-mediated magnetoelectric memory effect with Uni-axial $TbCo_2$/FeCo multilayer on 011-cut PMN-PT ferroelectric relaxor, J. Appl. Phys. **113**, 17C719 (2013).

[18] N. Tiercelin, Y. Dusch, A. Klimov, S. Giordano, V. Preobrazhensky, and P. Pernod, Room temperature magnetoelectric memory cell using stress-mediated magnetoelastic switching in nanostructured multilayers, Appl. Phys. Lett. **99**, 192507 (2011).

[19] J.-M. Hu and C.-W. Nan, Opportunities and challenges for magnetoelectric devices, APL Mater. **7**, 080905 (2019).

[20] A. Nicolenco, M. de h-Óra, C. Yun, J. MacManus-Driscoll, and J. Sort, Strain-gradient effects in nanoscale-engineered magnetoelectric materials, APL Mater. **9**, 020903 (2021).

[21] A. Dmitriyeva, V. Mikheev, S. Zarubin, A. Chouprik, G. Vinai, V. Polewczyk, P. Torelli, Y. Matveyev, C. Schlueter, I. Karateev, Q. Yang, Z. Chen, L. Tao, E. Y. Tsymbal, and A. Zenkevich, Magnetoelectric coupling at the $Ni/Hf_{0.5}Zr_{0.5}O_2$ interface, ACS Nano **15**, 14891 (2021).

[22] X. Liang, H. Chen, and N. X. Sun, Magnetoelectric materials and devices, APL Mater. **9**, 041114 (2021).

[23] S. González-Casal, I. Fina, F. Sánchez, and J. Fontcuberta, Direct reversible magnetoelectric coupling in a ferroelectric/ferromagnetic structure controlled by series resistance engineering, ACS Appl. Electron. Mater. **1**, 1937 (2019).

[24] S. Fan, H. Das, A. Rébola, K. A. Smith, J. Mundy, C. Brooks, M. E. Holtz, D. A. Muller, C. J. Fennie, R. Ramesh, D. G. Schlom, S. McGill, and J. L. Musfeldt, Site-Specific spectroscopic measurement of spin and charge in $(LuFeO_3)_m/(LuFe_2O_4)_1$ multiferroic superlattices, Nat. Commun. **11**, 5582 (2020).

[25] D. Pesquera, E. Khestanova, M. Ghidini, S. Zhang, A. P. Rooney, F. Maccherozzi, P. Riego, S. Farokhipoor, J. Kim, X. Moya, M. E. Vickers, N. A. Stelmashenko, S. J. Haigh, S. S. Dhesi, and N. D. Mathur, Large magnetoelectric coupling in multiferroic oxide heterostructures assembled via epitaxial lift-Off, Nat. Commun. **11**, 3190 (2020).

[26] Y. Liou, S. Ho, W. Tzeng, Y. Liu, P. Wu, J. Zheng, R. Huang, C. Duan, C. Kuo, C. Luo, Y. Chen, and J. Yang, Multiferroic materials: Extremely fast optical and nonvolatile control of mixed-phase multiferroic $BiFeO_3$ via instantaneous strain perturbation (Adv. mater. 5/2021), Adv. Mater. **33**, 2170035 (2021).

[27] P. Pahuja and R. P. Tandon, Latest advancement in magnetoelectric multiferroic composites, Ferroelectrics **569**, 108 (2020).

[28] A. Safin, V. Puliafito, M. Carpentieri, G. Finocchio, S. Nikitov, P. Stremoukhov, A. Kirilyuk, V. Tyberkevych, and A. Slavin, Electrically tunable detector of THz-frequency signals based on an antiferromagnet, Appl. Phys. Lett. **117**, 222411 (2020).

[29] E. T. Papaioannou and R. Beigang, THz spintronic emitters: A review on achievements and future challenges, Nanophotonics **10**, 1243 (2021).

[30] W. Wu, C. Yaw Ameyaw, M. F. Doty, and M. B. Jungfleisch, Principles of spintronic THz emitters, J. Appl. Phys. **130**, 091101 (2021).

[31] Y. Hirai, N. Yoshikawa, H. Hirose, M. Kawaguchi, M. Hayashi, and R. Shimano, Terahertz Emission From Bismuth Thin Films Induced by Excitation with Circularly Polarized Light, Phys. Rev. Appl. **14**, 064015 (2020).

[32] D. M. Nenno, L. Scheuer, D. Sokoluk, S. Keller, G. Torosyan, A. Brodyanski, J. Lösch, M. Battiato, M. Rahm, R. H. Binder, H. C. Schneider, R. Beigang, and E. T. Papaioannou, Modification of spintronic terahertz emitter performance through defect engineering, Sci. Rep. **9**, 13348 (2019).

[33] T. S. Seifert, in *Spintronics XIV*, edited by H.-J. M. Drouhin, J.-E. Wegrowe, M. Razeghi (SPIE, San Diego, California, USA, 2021), p. 28.

[34] B. Daneshmand, Analysis and evaluation of the effectiveness of methods for ensuring the quality of service for software-defined networks of the standard 5G/IMT-2020, Russ. Technol. J. **9**, 14 (2021).

[35] https://teraspintec.com/, (unpublished).

[36] https://www.tydexoptics.com/products/thz_optics/thz_waveplate/, (unpublished).

[37] Z. Feng, H. Qiu, D. Wang, C. Zhang, S. Sun, B. Jin, and W. Tan, Spintronic terahertz emitter, J. Appl. Phys. **129**, 010901 (2021).

[38] K. Cong, E. Vetter, L. Yan, Y. Li, Q. Zhang, Y. Xiong, H. Qu, R. D. Schaller, A. Hoffmann, A. F. Kemper, Y. Yao, J. Wang, W. You, H. Wen, W. Zhang, and D. Sun, Coherent control of asymmetric spintronic terahertz emission from Two-dimensional hybrid metal halides, Nat. Commun. **12**, 5744 (2021).

[39] D. Kong, X. Wu, B. Wang, T. Nie, M. Xiao, C. Pandey, Y. Gao, L. Wen, W. Zhao, C. Ruan, J. Miao, Y. Li,

and L. Wang, Broadband spintronic terahertz emitter with magnetic-field manipulated polarizations, Adv. Opt. Mater. **7**, 1900487 (2019).

[40] D. Khusyainov, S. Ovcharenko, M. Gaponov, A. Buryakov, A. Klimov, N. Tiercelin, P. Pernod, V. Nozdrin, E. Mishina, A. Sigov, and V. Preobrazhensky, Polarization control of THz emission using spin-reorientation transition in spintronic heterostructure, Sci. Rep. **11**, 697 (2021).

[41] O. Gueckstock, L. Nádvorník, T. S. Seifert, M. Borchert, G. Jakob, G. Schmidt, G. Woltersdorf, M. Kläui, M. Wolf, and T. Kampfrath, Modulating the polarization of broadband terahertz pulses from a spintronic emitter at rates up to 10 KHz, Optica **8**, 1013 (2021).

[42] H. Cheng, Q. Huang, H. He, Z. Zhao, H. Sun, Q. Wu, Z. Jiang, J. Wang, H. Huang, Z. Fu, and Y. Lu, Giant Electrical Modulation of Terahertz Emission in $Pb(Mg_{1/3}Nb_{2/3})_{0.7}Ti_{0.3}O_3$/Co-Fe-B/Pt Structure, Phys. Rev. Appl. **16**, 054011 (2021).

[43] See the Supplemental Material at http://link.aps.org/supplemental/10.1103/PhysRevApplied.17.044025 for the setup and sample description, the magnetization hysteresis loops, the dependence of the polarization rotation angle on the voltage, details about polarization measurements, the fitting procedure, and magnetization hysteresis loops.

[44] S. P. Kovalev and G. K. Kitaeva, Terahertz electro-optical detection: Optical phase or energy measurements, J. Opt. Soc. Am. B **30**, 2650 (2013).

[45] A. Buryakov, F. Zainullin, D. Khusyanov, D. Abdulaev, V. Nozdrin, and E. Mishina, Generation of elliptically polarized terahertz radiation from black phosphorus crystallites, Opt. Eng. **60**, 082013 (2021).

[46] M. Brunken, H. Genz, P. Gottlicher, C. Hessler, M. Huning, H. Loos, A. Richter, H. Schlarb, P. Schmuser, S. Simrock, D. Suetterlin, M. Tonutti, and D. Turke, Electro-optic sampling at the TESLA test accelerator: Experimental setup and first results, TESLA Rep. **11** (2003).

[47] A. Klimov, N. Tiercelin, V. Preobrazhensky, and P. Pernod, in *INTERMAG 2006 - IEEE International Magnetics Conference* (IEEE, 2006), pp. 452–452.

[48] N. Tiercelin, V. Preobrazhensky, V. Mortet, A. Talbi, A. Soltani, K. Haenen, and P. Pernod, Thin film magnetoelectric composites near spin reorientation transition, J. Magn. Magn. Mater. **321**, 1803 (2009).

[49] F. Wang, L. Luo, D. Zhou, X. Zhao, and H. Luo, Complete Set of elastic, dielectric, and piezoelectric constants of orthorhombic $0.71Pb(Mg_{1/3}Nb_{2/3})O_3$–$0.29PbTiO_3$ single crystal, Appl. Phys. Lett. **90**, 212903 (2007).

[50] S. Ovcharenko, M. Gaponov, A. Klimov, N. Tiercelin, P. Pernod, E. Mishina, A. Sigov, and V. Preobrazhensky, Photoinduced spin dynamics in a uniaxial intermetallic heterostructure $TbCo_2$/FeCo, Sci. Rep. **10**, 15785 (2020).

[51] B. J. Roxworthy and V. A. Aksyuk, Nanomechanical motion transduction with a scalable localized Gap plasmon architecture, Nat. Commun. **7**, 13746 (2016).

[52] S. Zhang, J. Wang, K. Hayashi, and F. Sassa, Monolithic processing of a layered flexible robotic actuator film for kinetic electronics, Sci. Rep. **11**, 20015 (2021).